

Effects of gaseous environments on physicochemical properties of thermally exfoliated graphene oxides for hydrogen storage: A comparative study

Sohan Bir Singh (✉ sohanbir@iitg.ac.in)

Indian Institute of Technology Guwahati <https://orcid.org/0000-0003-1376-6622>

Mahuya De

Indian Institute of Technology Guwahati

Manuscript

Keywords: Thermally exfoliated graphene oxide, Gaseous environment, Physicochemical properties, Hydrogen storage

Posted Date: February 4th, 2021

DOI: <https://doi.org/10.21203/rs.3.rs-170122/v1>

License: © ⓘ This work is licensed under a Creative Commons Attribution 4.0 International License.

[Read Full License](#)

Version of Record: A version of this preprint was published at Journal of Porous Materials on February 5th, 2021. See the published version at <https://doi.org/10.1007/s10934-021-01042-y>.

Effects of gaseous environments on physicochemical properties of thermally exfoliated graphene oxides for hydrogen storage: A comparative study

Sohan Bir Singh and Mahuya De*

Department of Chemical Engineering,

Indian Institute of Technology Guwahati

Guwahati, Assam 781039, India

Corresponding author's email – mahuya@iitg.ac.in

Tel.: +913612582270, Fax: +91 3612582291

Abstract

The present study compared the effect of different gaseous environments on physicochemical properties and subsequent hydrogen storage ability of thermally exfoliated graphene oxide (EGO). The reducing, inert or oxidizing environments were generated using hydrogen, argon or air as the carrier gas, respectively. The structure of thermally exfoliated graphene oxide depended on the type of gaseous environment. The EGO prepared in presence of Air showed the fluffiest layered structure having highest surface area. The surface area order was EGO(Air) ($268 \text{ m}^2/\text{g}$) > EGO(H_2) ($248 \text{ m}^2/\text{g}$) > EGO(Ar) ($155 \text{ m}^2/\text{g}$). The average pore sizes of EGO(Air) and EGO(H_2) were 2.9 and 2.8 nm, with pore volumes of 1.2 and 1.6 cm^3/g , respectively. The average pore size for EGO(Ar) was highest at 4.1 nm, associated with presence of larger void space and lowest total pore volume of 1.0 cm^3/g . Thus, presence of oxidative or reducing atmosphere seemed to be more conducive to exfoliation of layers by gradual removal of functional groups. The inert atmosphere of argon caused severe thermal separation of layers and functional groups, adversely affecting the layered structure as observed. The EGO(Air) also showed highest O/C ratio suggesting presence of significant amount of oxygen-containing functional groups on the surface. The hydrogen uptake order at 77 K and 30 bar was: EGO (Air) 3.34 wt.% > EGO (H_2) 3.12 wt.% > EGO (Ar) 2.2 wt.%. The highest uptake of EGO(Air) might have resulted from highest surface area, highest O/C ratio and presence of considerable pore volume.

Keywords: Thermally exfoliated graphene oxide; Gaseous environment; Physicochemical properties, Hydrogen storage

1 Introduction

Hydrogen is environmentally friendly and renewable source of energy [1-4]. Hydrogen has a gravimetric energy density of 142 MJ/kg which is three times higher compared to that of gasoline (~46.8 MJ/kg) [5, 6]. However, storage of hydrogen for utilization as an energy source has become one of the most challenging barriers [7-9]. The use of very high pressure and/or low temperature for conventional storage methods make them expensive and hazardous [10, 11]. Solid state storage of hydrogen is an alternative safe method. Carbon based materials, such as carbon fiber, templated carbon, activated carbon, carbon nanotube, with high surface area and large pore volume have been established as potential materials for hydrogen storage [12-16]. Both microporous and mesoporous carbons have been reported for hydrogen storage [17-25]. At 77 K, the hydrogen storage capacity has been reported in the range of 1.49–7.0 wt.% for pressure range of 20-100 bar and that at 298 K was reported in the range of 0.15-0.7 wt.% for 40-100 bar pressure [26-31]. Though the carbon-based materials have shown promising characteristics regarding hydrogen storage kinetics, however storage capacity and other properties are yet to reach the specifications recommended by the U.S. Department of Energy (DOE), which are accepted globally [32-34]. The supplementary Table S1 summarizes the specification of a hydrogen storage system for mobile application (light-duty vehicles) [35]. None of the developed solid storage systems till date have been able to satisfy all the conditions.

Graphene, an allotrope of carbon, is well known in the various field of applications, particularly sensors, gas storage, fuel cells, electrocatalysts and semiconductor [34, 36]. Recently, graphene has also generated interest as a potential hydrogen storage material [10, 34]. The graphene-based materials can be developed by different methods consisting of chemical, thermal and electrochemical treatment of graphite oxide [37–39]. The preparation of graphene like materials have been reported by using zeolite templated method [40]. The present paper focused on the graphene oxide prepared by exfoliation at high temperature in gaseous environments. The graphene with wide range of surface areas were reported (156–751 m²/g) on exfoliation in different gaseous environments in the temperature range of 523–2673 K [10, 12, 33, 37, 41–48]. The reported hydrogen storage at 77 K for graphenes, exfoliated in different carrier gases, also varied depending on the graphene properties and pressure used during adsorption (Supplementary Table S2). Wang et al. [12] reported the preparation of exfoliated sheets in flow of mixture of hydrogen and argon having the surface area of 300 m²/g. They obtained hydrogen uptake capacity of 1.75 wt.% at 54 bar. Lueking et al. [45] reported hydrogen uptake capacity of 1.2 wt.% at 20 bar for exfoliated graphite nanofibers prepared in presence of argon and

having surface area of 555 m²/g. Hudson et al. [47] observed 2.07 wt.% hydrogen uptake at 50 bar for thermally reduced graphene oxide (375 m²/g), exfoliated at 1323 K in presence of argon. At 100 bar, hydrogen uptake capacity of 3.0 wt.% was reported by Subrahmanyam et al. [48] for exfoliation of graphite oxide also prepared at 1323 K in the presence of argon. The corresponding surface area of this exfoliated graphene was reported as 925 m²/g. At room temperature the hydrogen uptake capacities of graphene oxides exfoliated in different gaseous environments were reported in the range of 0.10–0.49 wt.% at different pressures (20–90 bar) as shown in Supplementary Table S2 [12, 45, 47]. The corresponding surface areas were reported from 186 to 555 m²/g.

In the present study, the effects of reductive, oxidizing and inert gaseous environments on physical and chemical structures of thermally exfoliated graphene oxide were studied and compared. The corresponding effects on hydrogen storage properties was studied in detail by measuring hydrogen adsorption isotherms at different temperatures up to 30 bar. The literature survey showed that no systematic comparative studies, have done on the effect of different gaseous environments on the physicochemical properties of the thermally exfoliated graphene and their effect on the hydrogen storage properties to the best knowledge of the authors.

2 Experimental

2.1 Preparation

About 1 gm of graphite oxide (GO) (preparation described in Supplementary Fig. S1), taken in a quartz boat, was placed at the center of the horizontal reactor. The temperature of the sample was increased from 298 to 573 K in the flow of carrier gas, H₂, Ar or Air. The heating rate of 10 K/min was maintained. The desired temperature was determined initially by temperature programmed desorption (TPD) of GO in the respective carrier gas. The details are given in Supplementary Fig. S2. All the TPD profiles showed a peak in the range of 443–523 K, which may be attributed to the evolution of carbon oxides and water vapor originated from the removal of the oxygen-containing surface functional group [32]. These product gases along with the carrier gas can act as exfoliation agent for the GO samples resulting in multilayers graphene. Based on these results, the temperature of 573 K was selected as the exfoliation temperature for the samples in all carrier gases. The obtained thermally exfoliated graphene oxide samples were referred as EGO (H₂), EGO (Ar) and EGO (Air) corresponding to the carrier gas used for their preparation. The preparation sequence from graphite to GO to EGO samples is shown in Fig. 1.

2.2 Characterization

The physicochemical nature of the developed materials was established by the various characterization techniques. The presence of oxygen functional groups in the samples was investigated through FTIR spectroscopy (PerkinElmer–Frontier). The spectra were recorded in the wave number from 400 to 4000 cm^{-1} . The X–ray photoelectron spectroscopy (XPS) spectra were recorded using Thermo Fisher Scientific (ESCALAB) device with Al K α as the excitation source. The deconvolution of the XPS peaks was done by OriginPro 8.5 software. The baseline was corrected and fitting of the XPS peaks was done using the Gaussian method. The powder X–ray diffraction profiles were recorded between 5–70° using Bucker D8 advance diffractometer. The diffractometer was operated at 40 kV and 40 mA with Cu K α radiation. The approximate number of graphene layers was determined by equation 1 [32].

$$N_L = \frac{D_c}{d_{(002)}} + 1 \quad (1); \text{ The } N_L \text{ and } d_{(002)} \text{ represent number of layers and spacing between the layers,}$$

respectively. D_c , the average size of the graphitic zone, was calculated using Scherrer's formula

$$D_c = \frac{K\lambda}{\beta \cos \theta} \quad (2); \text{ A value of 0.9 was used for } K, \text{ the constant associated with crystallite shape factor. } \lambda$$

(nm) is the X–ray wavelength. The term β represented the broadness of the peak at half maximum. The surface area and pore size of materials were determined using a surface area analyzer (Quantachrome Autosorb iQ). At 77 K, the nitrogen isotherms were recorded. Before the surface area and pore analysis, the sample was degassed in helium atmosphere at 200 °C for 3 h. The surface area of the sample was calculated using Brunauer–Emmett–Teller (BET) method over the relative pressure range (P/P_0) of 0.05–0.30. The pore volume was determined up to 0.99. The pore size distributions (PSD) were determined by the non–local density functional theory (NLDFT) for slit pores. The degree of graphitization of the materials was characterized by Raman spectroscopy (Horiba jobin–Vyon T6400, Lab Raman HR) using radiation source of $\lambda = 514$ nm. Thermal stability of the samples was investigated by a thermogravimetric analyzer (TG, Netzsch). The heating rate was 10 K/min in nitrogen environment. The AFM images of samples were recorded in Agilent, 5500 series instrument. The height profile graph and average thickness were determined with the help of WSxM 5.0 Develop 8.2–Image browser software. The structural morphology of the materials was examined by the FESEM (Zeiss, Sigma 1430 VP) and TEM (JEM 2100, Make: JEOL). The elemental composition of the samples was determined by Energy Dispersive X–ray (EDX) unit attached to FESEM.

2.3 Hydrogen adsorption measurement

The hydrogen uptake capacity of samples was measured in a volumetric adsorption apparatus (Quantachrome iSorb–HP1–XKRLSPN100). A sample amount of about 100 mg was placed in the sample holder and degassed at 473 K for 3 h under ultrahigh vacuum to remove the unwanted gas and moisture present on the surface. The analysis temperature was controlled using an external bath circulator. The hydrogen adsorption–desorption isotherms were recorded using high–purity hydrogen (99.999 %) up to 30 bar at 77 K using a liquid nitrogen bath. The isosteric heat of adsorption of the samples was evaluated from the Clausius–Clapeyron equation using the adsorption isotherm data at 263 and 298 K. The equation is given as

$$Q_{ads} = R \left[\frac{d(\ln P)}{d(1/T)} \right]_q \quad (3)$$

Here isosteric heat of adsorption (Q_{ads}) is correlated to absolute temperature (T) and saturation pressure (P) of adsorption. R is the ideal gas constant. The slope of plot between (1/K) versus ln(P) at constant hydrogen adsorption (q) gives isosteric heat of adsorption.

3 Results and discussion

The compositions of all the sample as obtained from EDX analysis are summarised in Table 1. The graphite, used as starting material, contained 97.4 % carbon (Supplementary Fig. S3A). After oxidation, the oxygen content in the GO sample increased to 40.2 % (Table 1). GO had O/C ratio of 0.50 as obtained from EDX analysis (Supplementary Fig. S4). For EGO samples, the oxygen contents were in the range of 21.4 to 19.6 wt.% which corresponded to the O/C values between 0.18–0.20, depending on exfoliation environment. The removal of oxygen during exfoliation resulted in lower value of O/C ratio for EGO samples compared to that of GO. The oxygen removal was highest for EGO (Ar), resulting in O/C ratio 0.18 and least for EGO (Air) with highest O/C ratio of 0.20. For EGO (H₂), the O/C was 0.19. The removal of oxygen–containing functional groups was caused by decomposition or partial oxidation reactions involving these functional groups resulting in the evolution of CO/CO₂/H₂O during higher temperature treatments. The evolution of gases was confirmed by TPD analysis. The results suggested that removal of these functional groups depended to some extent on the environment of gases. In atmosphere of inert argon gas, the surface functional groups being only source of oxygen, their removal was highest while, in case of oxidative environment with presence of excess

oxygen, it was lowest. The EDX mapping (Supplementary Fig. S5) showed a denser oxygen distribution for GO. For all the exfoliated samples, the oxygen was observed to be more uniformly distributed on the surface, particularly for the air exfoliated sample.

The comparison of FTIR pattern of graphite, GO, EGO is shown in Fig. 2. The graphite showed peak due to C=C (1645 cm^{-1}) and hydroxyl group (3450 cm^{-1}) of adsorbed moisture. In addition to these two peaks, the two other peaks at 1377 and 1760 cm^{-1} were observed for GO sample which can be assigned to C–OH and C=O groups respectively, due to the generation of oxygen-containing groups on graphene surface [50, 51]. Since these two peaks were not observed for graphite, it confirmed the absence of oxygen-containing functional groups on its surface. In all the thermally exfoliated graphene oxide samples, similar peaks at 1377 , 1760 and 3450 cm^{-1} due to oxygen-containing functional groups were observed. The peak at 1645 cm^{-1} due to C=C was also observed in all the EGO samples.

The XPS spectra of the samples prepared by hydrogen and air exfoliation are shown in Fig. 3(A, B). Presence of C1s and O1s was detected. The oxygen peaks confirmed the presence of oxygen-containing surface functional groups. The C1s XPS spectra of samples were de-convoluted as shown in Fig. 3(C, E). Three peaks were obtained at 284.8 , 286.4 and 287.8 eV which may be assigned to C–C (sp^2 bonds), C–O (epoxy) and C=O (carbonyl) functional groups, respectively [34, 53]. The presence of oxygen-containing functional groups in the EGO (H_2) and EGO (Air) samples was also confirmed by O1s peaks and the corresponding deconvolution of the peaks is shown in Fig. 3(D, F). The peak assigned to carbonyl group, C=O, was observed at 531.5 eV and the peak at 533.5 eV corresponded to C–O, the epoxy group [53, 54]. The peak at 537.7 eV can be attributed to the presence of C–OH (hydroxyl) group [55–57]. The areas under the peaks are shown in Supplementary Table S3. It can be observed that for both the samples, relative distributions of the three types of oxygen containing functional groups were similar with carbonyl oxygen being present in highest amount closely followed by epoxy oxygen. The presence of hydroxyl oxygen was lowest. It can be further observed that for EGO (Air), the amount of all the three types of oxygen containing–functional groups were higher compared to that of EGO (H_2) rendering total oxygen content of former also higher. The ratio of carbonyl oxygen to epoxy oxygen was higher for EGO (Air) compared to that of EGO (H_2). The ratios were 1.052 and 1.015 for EGO (Air) and EGO (H_2), respectively. Both the samples also showed higher epoxy relative to hydroxyl content. The ratios of epoxy to hydroxyl content were 1.45 and 1.47 for EGO (H_2) and EGO (Air), respectively. Thus, the relative epoxy content was higher for EGO (Air). The O/C ratios calculated from XPS analysis gave the values of 0.19 and 0.20 for

EGO (H₂) and EGO (Air), respectively. These values of O/C ratio agreed well with that obtained from EDX analysis of these samples.

Fig. 4 shows the XRD profiles of samples. The corresponding lattice spacing, crystal size and number of layers are tabulated in Table 2. The high-intensity peak was observed at $2\theta = 26.5^\circ$ for graphite, corresponding to the hexagonal graphitic plane (002) with a d-spacing of 0.337 nm [10]. After oxidation to GO, the peak corresponding to C(002) plane shifted to $2\theta = 10.4^\circ$. The d-spacing of C(002) planes increased from 0.337 nm for graphite to 0.850 nm for GO. The expansion of d-spacing agreed with the intercalation of oxygen groups within the graphene layers [53]. The intensity of the peak decreased compared to starting graphite, suggesting the drop in crystallinity caused by the separation of graphitic layers. All the exfoliated samples exhibited a broad peak at $2\theta = 24.5^\circ$ corresponding to graphitic zone. The corresponding d-spacing values were 0.381, 0.372, and 0.364 nm for EGO exfoliated in Air, H₂, and Ar, respectively. This reduction in d-spacing for all the EGO samples compared to that of GO may be associated with the elimination of intercalated oxygen-containing functional groups. Higher the removal of functional groups during exfoliation lower should be the layer separation. The lowest value of d-spacing for EGO (Ar) may be associated with most effective removal of functional groups in inert condition of argon. This agreed well with the lowest oxygen content as observed from EDX analysis of the sample. The highest separation of layers for EGO (Air) also agreed with the presence of highest amount of intercalated oxygen-containing functional groups as observed from EDX and XPS analyses. The number of layers of the samples as determined from equation 2, was in the range of 2–5.

Fig. 5 shows the tapping-mode AFM topography images with height profile analysis for EGO samples. The average thickness and number of layers are summarised in Table 2. The average thickness of thermally exfoliated samples was in 3.5–3.8 nm range. This corresponded to approximately 8–9 number of graphene layers. The number of graphene layers was calculated from the average thickness values, using the reported theoretical thickness of 0.40 nm for single graphene layer [55, 56].

The morphology of the samples was studied using FESEM (Fig. 6) and TEM (Fig. 7). The morphology of graphite showed heterogeneous thick stacks (Supplementary Fig. S3B). TEM image clearly showed a dense structure (Supplementary Fig. S3C). After oxidation, change in morphology can be observed in the corresponding FESEM and TEM images. The sample structure significantly changed on exfoliation. The exfoliated samples had fluffier layered

structure which might have resulted from the better separation of layers. The separation might have been assisted by the formation of gaseous products and gas flow as discussed earlier. For all the EGO samples, the large pores were observed from FESEM images, which might have resulted from thermal degradation of layers. The comparison of the images suggested that in different exfoliation atmosphere, the formation of the layered structure differed. The layered structure seemed to be most well developed in Air atmosphere leading to its highest surface area.

The nitrogen adsorption–desorption isotherms obtained at 77 K for GO and different graphene samples are shown in Fig. 8A. For GO, the type–II isotherm with H4 hysteresis loop indicated the presence of slit–shaped pores, same as that for graphite (Fig. S3D). All the gas exfoliated samples showed type–IV isotherm with a dominant H4 hysteresis loop suggesting strong mesoporous nature with the presence of narrow slit–shaped pores [10]. Change from type II to type IV isotherm after exfoliation suggested significant structural changes. Though the nature of the isotherm did not change significantly with change in gaseous environment, however the nitrogen adsorption was lowest for sample prepared in argon and highest for sample prepared in Air.

The corresponding BET surface area and pore volume of samples are summarized in Table 3. The graphite had a surface area of 14 m²/g which increased to 33 m²/g after oxidation. This increase of surface area may be attributed to layer separation by incorporation of oxygen–containing functional groups. However, total pore volume was not much affected. The exfoliation in the presence of different gases increased the surface area and pore volume drastically. The increase in surface area and pore volume depended on the nature of gaseous environment during the exfoliation of GO. The thermally exfoliated graphene oxide prepared in the presence of Air had a higher surface area (268 m²/g) followed by that of H₂ (248 m²/g) and Ar (155 m²/g). The pore volume order of exfoliated samples is EGO (H₂), 1.6 cm³/g > EGO (Air), 1.2 cm³/g > EGO (Ar), 1.0 cm³/g. The well–developed layered structure for Air exfoliated samples may have led to its highest surface area. The lowest surface area and pore volume of EGO (Ar) might have resulted from major modification of layered structure in an inert atmosphere as observed in other characterization results. The micropore area and volume were negligible for all the EGO samples agreeing with their mainly mesoporous character. The pore size distributions of the samples are shown in Fig. 8B. The graphite had pores in the broad range of 0.8 to 30 nm (Supplementary Fig. S3E) with very low pore volume and, the oxidized sample GO showed pores in the range of 0.5 to 3 nm (Fig. 8B inset). The pores of exfoliated samples were mainly situated in mesoporous range; H₂ and Air

exfoliated samples had pores in the range of 1.8 to 6 nm, while the Ar exfoliated sample had in 3.6 to 7 nm range. The average pore size of H₂ and air exfoliated graphene were 2.8 and 2.85 nm, respectively as can be observed from Table 3. The highest average pore size of 4.1 nm observed for EGO (Ar) suggested more extensive modification in the layered structure. This mesoporous structure for all the exfoliated samples may have originated from the better separation of layers during exfoliation as observed from FESEM images. The comparison of results suggests that presence of oxidative or reducing atmosphere was more conducive to exfoliation of layers by gradual removal of functional groups. The removal might have been assisted by atmosphere promoting mild oxidation or reduction reactions. The inert atmosphere of argon may have caused more severe thermal separation of layers and functional groups. This adversely affected the layered structure and generated larger void spaces and which in turn resulted in lowest total surface area and highest pore size for EGO (Ar) as observed.

Fig. 9 shows the Raman spectra of the samples in the range of 500 to 3000 cm⁻¹. In the Raman spectrum of graphite, the G band peak was observed at 1582 cm⁻¹ (Supplementary Fig. S3F). The 2D band appeared at 2726 cm⁻¹ and this second order of D band corresponded to two-phonon lattice vibrational process [39]. For GO and various EGO samples, the peak for D band was observed in the wave number range of 1344 to 1356 cm⁻¹ due to the defects present in the samples [40]. The defect in GO resulted from the incorporation of functional groups. The appearance of D-band in graphene samples may be associated with the additional modifications incorporated during thermal exfoliation of GO. The G band appeared in the range 1589 to 1600 cm⁻¹ for GO and graphene samples. The G band is attributed to in-plane bond stretching vibration of sp² bonded carbon atoms within layers. For GO, a larger intensity of D and G bands compared to that of graphene samples suggested that the GO had more disorder in its structure and more distortion of carbon layers. It may be attributed to the existence of the intercalated oxygen-containing functional group in the GO. The I_D/I_G intensity ratio values corresponding to D and G bands of the samples are tabulated in Table 2. The GO exhibited highest I_D/I_G ratio of 0.98 in accordance with most distortion in structure. The exfoliation which caused partial removal of intercalated functional groups resulted in decrease in I_D/I_G ratio for all the thermally exfoliated graphene samples compared to that of GO suggested partial restoration of graphitic zone. The lowest value of I_D/I_G was 0.90 for EGO (Air) sample, which indicated the presence significant amount of graphitic zone in the sample. The highest I_D/I_G value of 0.94 for EGO (Ar) suggested the presence of least amount of graphitic zone in the sample which agreed with more thermal distortion of layers in inert atmosphere.

The Thermogravimetric analysis (TGA) and Differential Thermogravimetric (DTG) profiles of the samples are shown in Fig. 10(A, B). The graphite was stable up to 1023 K, thereafter 4 wt.% mass loss was observed till 1173 K. For the oxidized GO sample, the weight loss of ~19 wt.% was observed below 393 K, which may be attributed to the removal of moisture. Thereafter, rapid mass loss of about 26 wt.% in the range of 433 to 553 K corresponded to the elimination of oxygen-containing functional groups [37]. After 553 K, the GO sample underwent further gradual weight loss of 19 wt.% up to 1173 K, suggesting further removal of different functional groups and as well as carbons in the form of carbon oxides. For the EGO samples the weight loss was initiated only after 773 K and peaks were observed beyond 900 K. The presence of these high temperature peaks suggested presence of only strongly bounded oxygen-containing functional groups in EGO samples that were not removed during exfoliations done at 573 K. These strongly bonded functional groups on surface, retained even after the exfoliation, were removed only at a higher temperature as observed. The peak for EGO (Air) was observed at highest temperature at 1075 K suggesting presence of most strongly bounded functional groups. This was also reflected in their mass loss values. The Air, H₂ and Ar exfoliated graphene oxide samples showed mass loss of 33, 40 and 44 %, respectively, up to 1173 K. The EGO (Air) sample, inspite of having highest O/C ratio, showed lowest weight loss suggesting retainment of functional groups even in high temperature of TGA. The order of mass loss suggested that functional groups were most strongly bonded to the surface of EGO (Air) followed by that of EGO (H₂) and least in EGO (Ar).

3.1 Hydrogen uptake

Fig. 11(A, B) compares the hydrogen adsorption isotherms of the GO and EGO samples. The isotherms were recorded at 77 K up to 1, 30 and 60 bar. The hydrogen isotherm obtained in this study agreed with many studies reported for graphene-based materials. At lower pressure it showed typical convex nature corresponding to strong adsorbent force field and stronger molecular interaction (Fig. 11A). But at higher pressure, rate of hydrogen uptake was lowered and uptake increased more gradually (Fig. 11B), as also reported by others [45, 47]. At further higher pressure of 50-60 bar, the hydrogen uptake reduced further (Supplementary Fig. S6). The gradual decrease in hydrogen uptake at higher pressure may be explained by reduced effectiveness of force field of adsorbent and filled up pore volumes with increased layers of adsorbate at higher pressure.

The GO had the lowest hydrogen uptake (1.09 wt.%). The reason may be its very low surface area and pore volume (Table 3). The hydrogen uptake values of the EGO samples at 77 K and 30 bar are compared in Table 3. The order of hydrogen uptake was EGO (Air), 3.34 wt.% > EGO (H₂), 3.12 wt.% > EGO (Ar), 2.2 wt.%.

The hydrogen storage for graphene materials occurs by physical adsorption involving Vander Waal's forces between surface and hydrogen molecules [57]. Hence, the available surface area is a determining factor for extent of adsorption. The next most important parameter is the pore size and pore volume, determining the extent of multilayer adsorption possible within the pores. The third major determining parameter in adsorption process is the presence of other heteroatoms, which may provide additional interaction sites for adsorbate molecule on the surface. In this case, the presence of highly electronegative oxygen in form of surface functional groups may have also contributed towards interaction with highly electropositive hydrogen molecules. Various studies have also reported that the presence of oxygen-containing surface functional in carbon based materials facilitated hydrogen uptake phenomena [59–61]. The highest hydrogen uptake for EGO (Air) may be attributed highest surface area. Fig. 11C shows linear increase in hydrogen uptake with increasing surface area of the samples. The highest oxygen content of EGO (Air) also may have facilitated hydrogen uptake. Similarly, lowest uptake observed for EGO (Ar) may be attributed to its lowest surface area, pore volume and oxygen content. The hydrogen uptake values obtained in this study are at par or better than that reported for exfoliated graphene like samples (Supplementary Table S2). For graphene prepared by zeolites templated method the hydrogen uptake was higher due to very high surface area, but hydrogen uptake per unit surface area was much better for samples prepared in present study. The higher hydrogen uptake per unit area for present study might have been facilitated by presence of oxygen heteroatom on the graphene surface. Higher presence of surface oxygen in exfoliated samples might also be the reason for their higher hydrogen uptake compared to hydrazine reduced graphene oxide sample in spite of higher surface area of the latter.

The room temperature hydrogen uptake of the samples was measured at 298 K up to 30 bar. The hydrogen adsorption isotherms are shown in Fig. S7A in Supplementary. The hydrogen uptake capacity was much lower at this temperature (0.10–0.22 wt.%) compared to that measured in 77 K. As the hydrogen uptake was low at room temperature, the isotherms showed convex nature for entire pressure range studied. The lower hydrogen uptake at room temperature compared to that at 77 K agreed with the physisorption mechanism. According to physisorption mechanism with increase in temperature, the multiple layers of physically adsorbed hydrogen reduces, thereby lowering the hydrogen

uptake. The hydrogen uptake at 298 K followed the same increasing trend with surface area as was observed at 77 K (Supplementary Fig. S7B).

The isosteric heat of adsorption of the samples is shown in Fig. 11D. The heat of adsorption decreased with increasing hydrogen uptake for all the samples. At lower hydrogen adsorption, the order of heat of adsorption in kJ/mol was EGO(Ar), 7.2 < EGO(H₂), 8.5 < EGO (Air), 8.9, which at higher adsorption decreased to the range of 3–4 kJ/mol. This decrease is the result of the initial occupation of stronger sites by hydrogen on the graphene surface, followed by adsorption on comparatively weaker sites (weak binding energy). The variation in the heat of adsorption among the samples at lower uptake suggested difference in the interaction of hydrogen with the sample surface. The less variation of the heat of adsorption for samples at higher uptake suggested that the residual weaker sites were similar in nature for all the graphene oxide samples prepared in different environments. The heat of adsorption (4–9 kJ/mol) obtained in this study is slightly higher than that reported in the literature (3–6 kJ/mol) [62].

3.2 Cyclic stability

The EGO (Air) showing the highest hydrogen uptake was further subjected to cyclic stability test at 77 K and 30 bar. The hydrogen adsorption and desorption cycles were repeated 5 times for the same sample and the corresponding profiles are shown in Fig. 12(A, B). The desorption curve followed the same path as the adsorption curve for all the cycles indicating a completely reversible hydrogen adsorption process. The hydrogen uptake capacity decreased only slightly with the number of cycles. After 5 cycles, the hydrogen uptake decreased from initial value of 3.34 to 3.02 wt.%, corresponding to about 9 % reduction from the original value. This indicated a good cyclic stability of the EGO (Air) sample as a hydrogen uptake material. The slight decrease in hydrogen uptake capacity after 5 cycles may be attributed mainly to lowering of surface area and pore volume (Supplementary Fig. S8). The lowering of these values, in turn, may have caused by the partial damage of layers or collapse of porous structure (Supplementary Fig. S8) due to cyclic exposure at higher pressure. In spite of slight modification of the porous structure of the sample, the hydrogen uptake stability was observed to be good for the present sample. Only limited studies have reported cyclic stability of graphene based sample for hydrogen uptake. Klechikov et al. [63] reported 44 % drop in hydrogen uptake for Pd doped exfoliated graphene oxide after 4 cycles. But the same author reported only 2.5 % reduction after 5 cycles for KOH activated graphene [63].

4 Conclusions

The present study compared the effect of different gaseous environments on physicochemical properties and subsequent hydrogen storage ability of thermally exfoliated graphene oxide. The exfoliation was carried out in three different gaseous environments. A reducing, inert or oxidizing environments were generated using hydrogen, argon or air as the carrier gas, respectively. All the exfoliated samples were mesoporous in nature, having fluffy and distinct multi-layered structure. However, nature of the layered structure depended on the gaseous environment. The EGO sample prepared in presence of Air, showed the fluffiest layered structure resulting in highest surface area. The BET surface area order was EGO(Air) (268 m²/g) > EGO(H₂) (248 m²/g) > EGO(Ar) (155 m²/g). The average pore size for EGO(Ar) was highest at 4.1 nm, suggesting presence of larger void space. This also resulted in its lowest total pore volume of 1.0 cm³/g. The average pore size of EGO(Air) and EGO(H₂) were 2.9 and 2.8 nm, while pore volumes were 1.2 and 1.6 cm³/g, respectively. The results suggested that the presence of oxidative or reducing atmosphere was more conducive to exfoliation of layers by gradual removal of functional groups. The inert atmosphere of argon might have caused more severe thermal separation of layers and functional groups adversely affecting the layered structure. This generated larger void spaces resulting in its lowest total surface area and highest pore size as observed. The EGO (Air) also showed the highest O/C ratio suggesting presence of significant amount of oxygen-containing functional groups on the surface. The hydrogen uptake order at 77 K and 30 bar was EGO(Air) 3.34 wt.% > EGO(H₂) 3.12 wt.% > EGO(Ar) 2.2 wt.%. The highest uptake of EGO (Air) may have resulted from highest surface area, highest O/C ratio and presence of considerable pore volume.

Acknowledgments

The authors gratefully acknowledge the Central Instruments Facility (CIF), Indian Institute of Technology Guwahati and DST-FIST India (SR/FST/ETII-028/2010) for providing instrumentation facilities.

References

1. A. Klechikov, G. Mercier, P. Merino, S. Blanco, C. Merino, A. Talyzin, *Microporous Mesoporous Mater.* **210**, 46–51 (2015).
2. M. Ohno, N. Okamura, T. Kose, T. Asada, K. Kawata, J. *Porous Mater.* **19**, 1063–1069 (2012).
3. H. Zhou, J. Zhang, J. Zhang, X. Yan, X. Shen, A. Yuan, *Int. J. Hydrogen Energy* **40**, 12275–12285 (2015).
4. M. Chen, X. Xiao, M. Zhang, J. Mao, J. Zheng, M. Lui, X. Wang, L. Chen, *Mater. Today Energy* **16**, 100411 (2020).

5. B. Kim, W. Hong, H. Yu, Y. Han, S. Lee, S. Chang, *Phys. Chem. Chem. Phys.* **14**, 1480–1484 (2012).
6. V. Jain, B. Kandasubramanian, *J. Mater. Sci.* **55**, 1865–1903 (2020).
7. X. Liu, Y. Wu, S. Wang, Z. Li, X. Guo, J. Ye, *J. Mater. Sci.* **55**, 2645–2660 (2020).
8. Y. Liu, D. Li, B. Lin, Y. Sun, X. Zhang, H. Yang, *J. Porous Mater.* **22**, 1417–1422 (2015).
9. E. Gkanas, A. Damian, A. Ioannidou, G. Stoian, N. Lupu, M. Gjoka, S. Makridis, *Mater. Today Energy* **13**, 186–194 (2019).
10. P. Divya, S. Ramaprabhu, *Phys. Chem. Chem. Phys.* **16**, 26725–26729 (2014).
11. J. Hassan, C. Guthrie, G. Diamantopoulos, E. Reardon, *Mater. Today Energy* **4**, 1–6 (2017).
12. Q. Zheng, X. Ji, S. Gao, X. Wang, *Int. J. Hydrogen Energy* **38**, 10896–10902 (2013).
13. Y. Liu, Z. Zhang, T. Wang, *Int. J. Hydrogen Energy* **43**, 11120–11131 (2018).
14. S. Singh, M. De, *Microporous Mesoporous Mater.* **257**, 241–252 (2018).
15. L. Ma, Z. Wu, J. Li, E. Wu, W. Ren, H. Cheng, *Int. J. Hydrogen Energy* **34**, 2329–2332 (2009).
16. L. Molefe, N. Musyoka, J. Ren, H. Langmi, P. Ndungu, R. Dawson, *J. Mater. Sci.* **54**, 7078–86 (2019).
17. R. J. Konwar, M. De, *Int. J. Energy Res.* **39**, 223–233 (2015).
18. R. J. Konwar, M. De, *J. Anal. Appl. Pyrolysis* **107**, 224–232 (2014).
19. S. B. Singh, M. De, *Int. J. Energy Res.* **43**, 4264–4280 (2019).
20. S. B. Singh, M. De, *Mater. Chem. Phys.* **239**, 122102 (2020).
21. H. Nishihara, P.-X. Hou, L.-X. Li, M. Ito, M. Uchiyama, T. Kaburagi, A. Ikura, J. Katamura, T. Kawarada, K. Mizuuchi, *J. Phys. Chem. C* **113**, 3189–3196 (2009).
22. N. P. Stadie, J. J. Vajo, R. W. Cumberland, A. A. Wilson, C. C. Ahn, B. Fultz, *Langmuir* **28**, 10057–10063 (2012).
23. A. J. Lachawiec Jr, R. T. Yang, *Langmuir* **24**, 6159–6165 (2008).
24. H. Nishihara, F. Ohtake, A. Castro-Muñiz, H. Itoi, M. Ito, Y. Hayasaka, J. Maruyama, J. N. Kondo, R. Osuga and T. Kyotani, *J. Mater. Chem. A* **6**, 12523–12531 (2018).
25. H. Nishihara, T. Simura and T. Kyotani, *Chem. Commun.* **54**, 3327–3330 (2018).
26. Q. Zheng, X. Ji, S. Gao, X. Wang, *Int. J. Hydrogen Energy* **38**, 10896–10902 (2013).
27. C. Guan, X. Zhang, K. Wang, C. Yang, *Sep. Purif. Technol.* **66**, 565–569 (2009).
28. N. Alam, R. Mokaya, *Microporous Mesoporous Mater.* **144**, 140–147 (2011).
29. H. Nishihara, T. Simura, T. Kyotani, *Chem. Commun.* **54**, 3327 (2018).
30. N.F. Attia, S.M. Lee, H.J. Kim, K.E. Geckeler, *Microporous Mesoporous Mater.* **173**, 139–146 (2013).
31. Y. Xia, R. Mokaya, *J. Phys. Chem. C* **111**, 10035–10039 (2007).
32. C. Zhou, J. Szpunar, *ACS Appl. Mater. Interfaces* **8**, 25933–259408 (2016).
33. I. Toda, K. Komatsu, T. Watanabe, H. Toda, H. Akasaka, S. Ohshio, H. Saitoh, *J. Porous Mater.* **25**, 1765–1770 (2018).
34. S. Gadipelli, Z. Guo, *Prog. Mater. Sci.* **69**, 1–60 (2015).
35. D. Anton, T. Semelsberger, D. Siegal, K. Brooks and B. Hardy, (energy.gov, 2013).
36. X. Hu, Y. Yu, Y. Wang, J. Zhou, L. Song, *Appl. Surf. Sci.* **329**, 83–86 (2015).

37. C. Botas, P. Alvarez, C. Blanco, R. Santamaría, M. Granda, M.D. Gutiérrez, *Carbon* **52**, 476–485 (2013).
37. Y. Cui, R. Zhang, J. Zhang, Z. Wang, H. Xue, W. Mao, W. Huang, *Mater. Today Energy* **7**, 44–50 (2018).
39. I. Moon, J. Lee, R. Ruoff, H. Lee, *Nat. Commun.* **1**, 73 (2010).
40. H. Nishihara, T. Kyotani, *Chem. Commun.* **54**, (2018) 5648.
41. A. Abdelkader, A. Cooper, R. Dryfe, I. Kinloch, *Nanoscale* **7**, 6944–6956 (2015).
42. V. Parambath, R. Nagar, K. Sethupathi, S. Ramaprabhu, *J. Phys. Chem. C* **115**, 15679–15685 (2011).
43. G. Srinivas, J. Burrell, J. Ford, T. Yildirim, *J. Mater. Chem.* **21**, 11323–11329 (2011).
44. Z. Wu, W. Ren, L. Gao, B. Liu, C. Jiang, H.M. Cheng, *Carbon* **47**, 493–499 (2009).
45. A. Lueking, L. Pan, D. Narayanan, C. Clifford, *J. Phys. Chem. B* **109**, 12710–12717 (2005).
46. W. Hong, B. Kim, S. Lee, H. Yu, Y. Yun, Y. Jun, *Int. J. Hydrogen Energy* **37**, 7594–7599 (2012).
47. M. Hudson, H. Raghubanshi, S. Awasthi, T. Sadhasivam, A. Bhatnager, S. Simizu, *Int. J. Hydrogen Energy* **39**, 8311–8320 (2014).
48. K. Subrahmanyam, S. Vivekchand, A. Govindaraj, C. Rao, *J. Mater. Chem.* **18**, 1517–1523 (2008).
49. N. Balahmar, A. M. Lowbridge and R. Mokaya, *J. Mater. Chem. A* **4**, 14254–14266 (2016).
50. Z. Tang, L. Zhang, C. Zeng, T. Lin, B. Guo, *Soft Matter*. **8**, 9214–9220 (2012).
51. A. Das, M. Srivastav, R. Layek, M. Uddin, D. Jung, N. Kim, *J. Mater. Chem. A* **2**, 1332–1340 (2014).
52. I. Kottegoda, X. Gao, L. Nayanajith, C. Manorathne, J. Wang, J. Wang, *J. Mater. Res. Technol.* **31**, 907–912 (2015).
53. C. Chen, T. Chung, C. Shen, M. Yu, C. Tsao, G. Shi, *Int. J. Hydrogen Energy* **38**, 3681–3688 (2013).
54. S. Chowdhury, R. Balasubramanian, *J. CO2 Util.* **13**, 50–60 (2016).
55. S. Stankovich, D. Dikin, G. Dommett, K. Kohlhaas, E. Zimney, E. Stach, *Nature* **442**, 82 (2006).
56. N. Pu, C. Wang, Y. Sung, Y. Liu, M. Ger, *Mater. Lett.* **63**, 1987–1989 (2009).
57. V. Tozzini, V. Pellegrini, *Mater. Lett.* **15**, 80–89 (2013).
58. C. Zhou, J. Szpunar, X. Cui, *ACS Appl. Mater. Interfaces* **8**, 15232–15241 (2016).
59. R. Rajaura, S. Srivastava, V. Sharma, P. Sharma, C. Lal, M. Singh, *Int. J. Hydrogen Energy* **41**, 9454–9461 (2016).
60. H. Shiraz, O. Tavakoli, *Renew. Sustain. Energy Rev.* **74**, 104–109 (2017).
61. L. Wang, F. Yang, R. Yang, M. Miller, *Ind. Eng. Chem. Res.* **48**, 2920–2926 (2009).
62. G. Srinivas, Y. Zhu, R. Piner, N. Skipper, M. Ellerby, R. Ruoff, *Carbon* **48**, 630–635 (2010).
63. A. Klechikov, G. Mercier, T. Sharifi, I. Baburin, G. Seifert, A. Talyzin, *Chem. Commun.* **51**, 15280–15283 (2015).

Figures

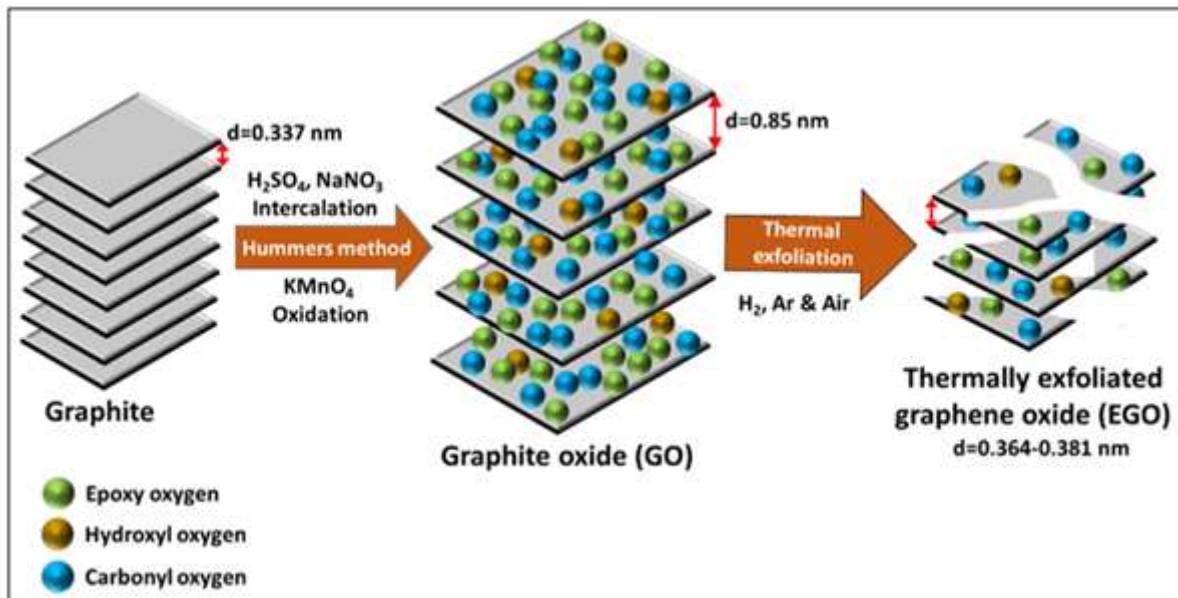


Figure 1

Preparation sequence of graphite oxide (GO) and thermally exfoliated graphene oxide (EGO) from graphite.

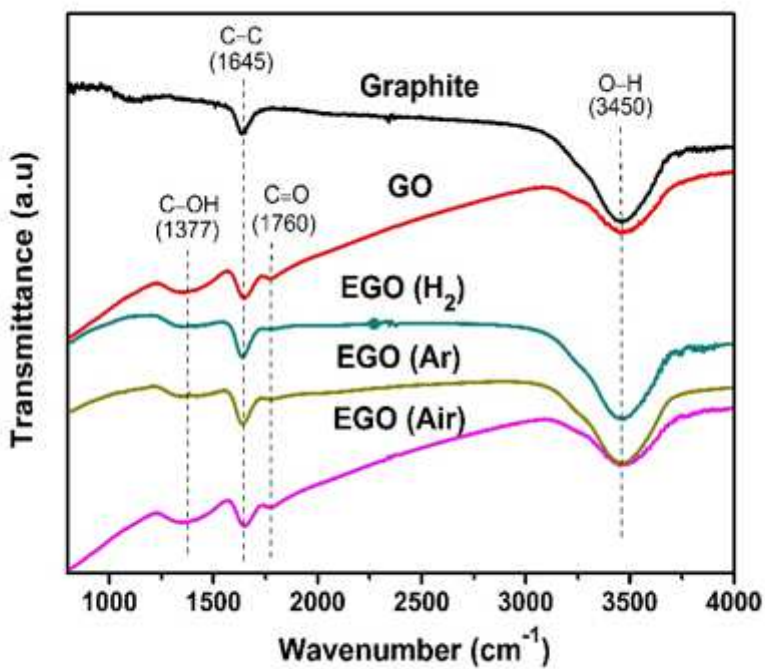


Figure 2

FTIR profiles of graphite, graphite oxide (GO) and thermally exfoliated graphene oxide (EGO) samples in H₂, Ar or Air environments.

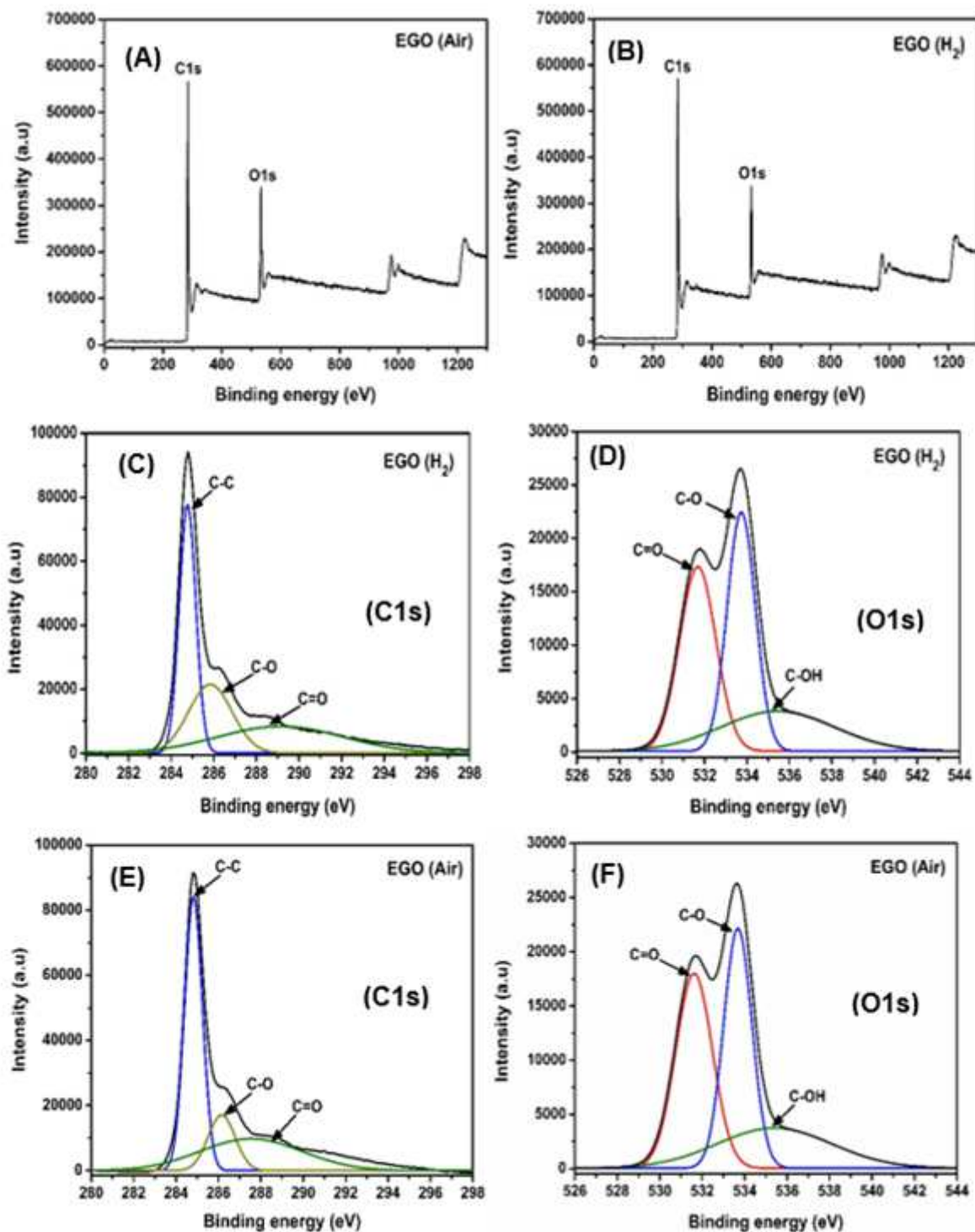


Figure 3

Overall XPS surface survey spectrum of (A) EGO (H₂), (B) EGO (Air), C1s and O1s XPS spectra of (C, D) EGO (H₂) and (E, F) EGO (Air).

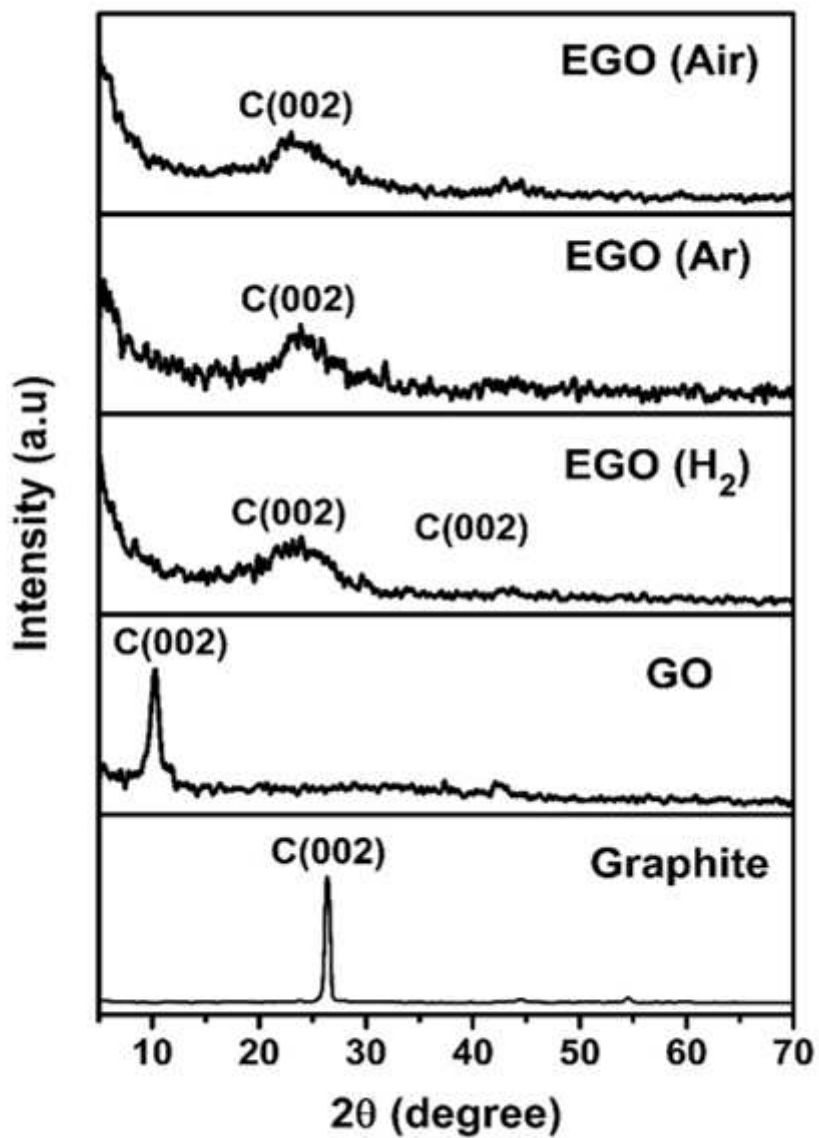


Figure 4

XRD patterns of graphite, graphite oxide (GO) and thermally exfoliated graphene oxide (EGO) samples in H₂, Ar or Air environments.

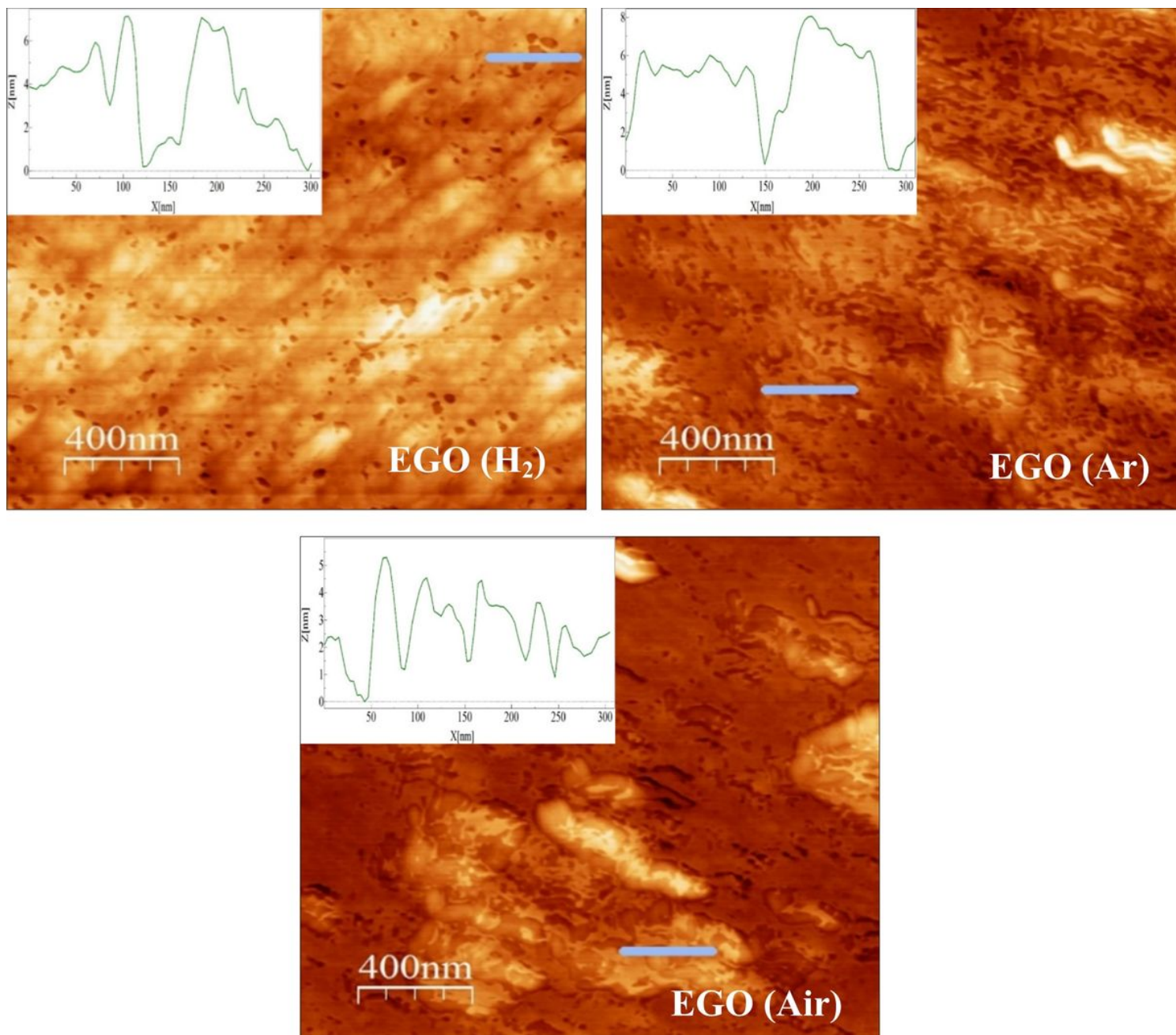


Figure 5

AFM images with corresponding height profiles of thermally exfoliated graphene oxide (EGO) samples in H₂, Ar or Air environments.

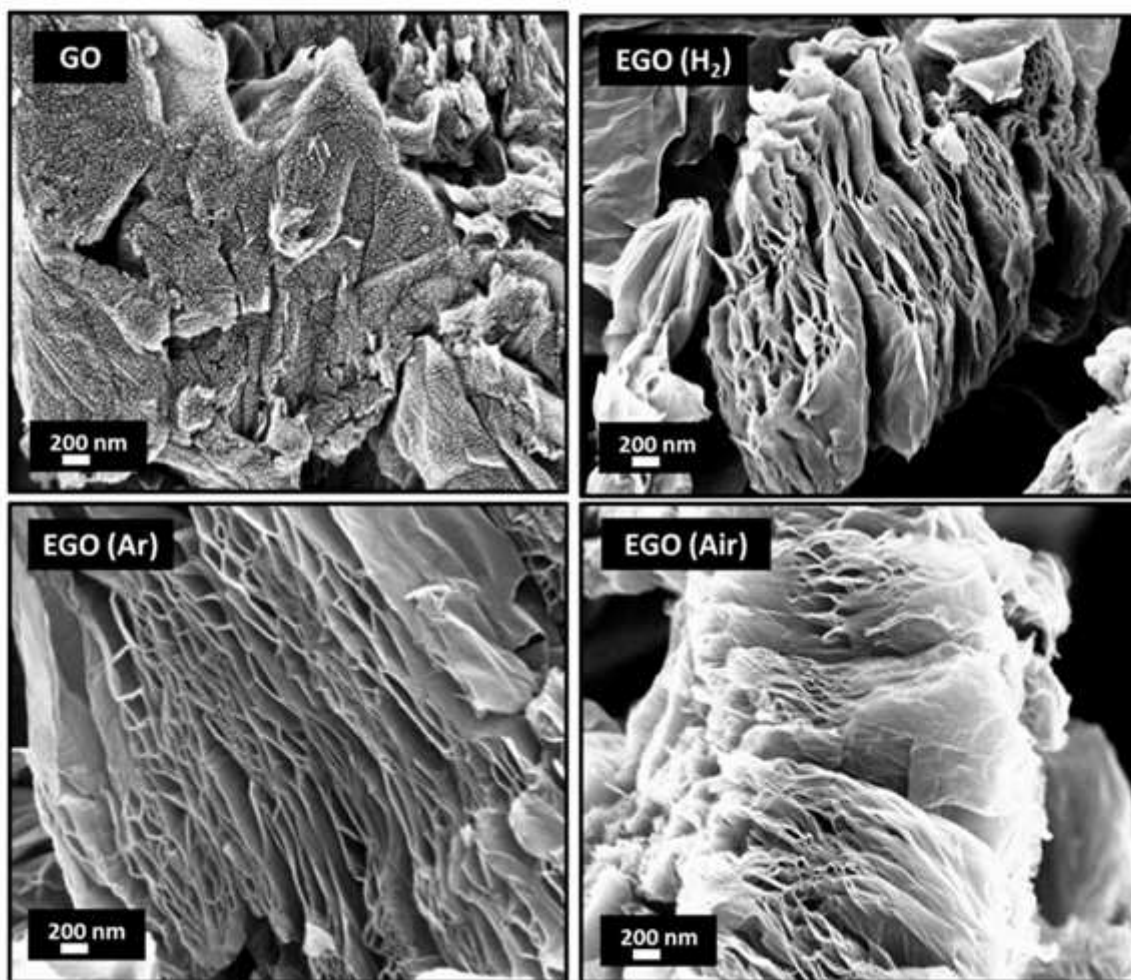


Figure 6

FESEM images of graphite oxide (GO) and thermally exfoliated graphene oxide (EGO) samples in H₂, Ar or air environments.

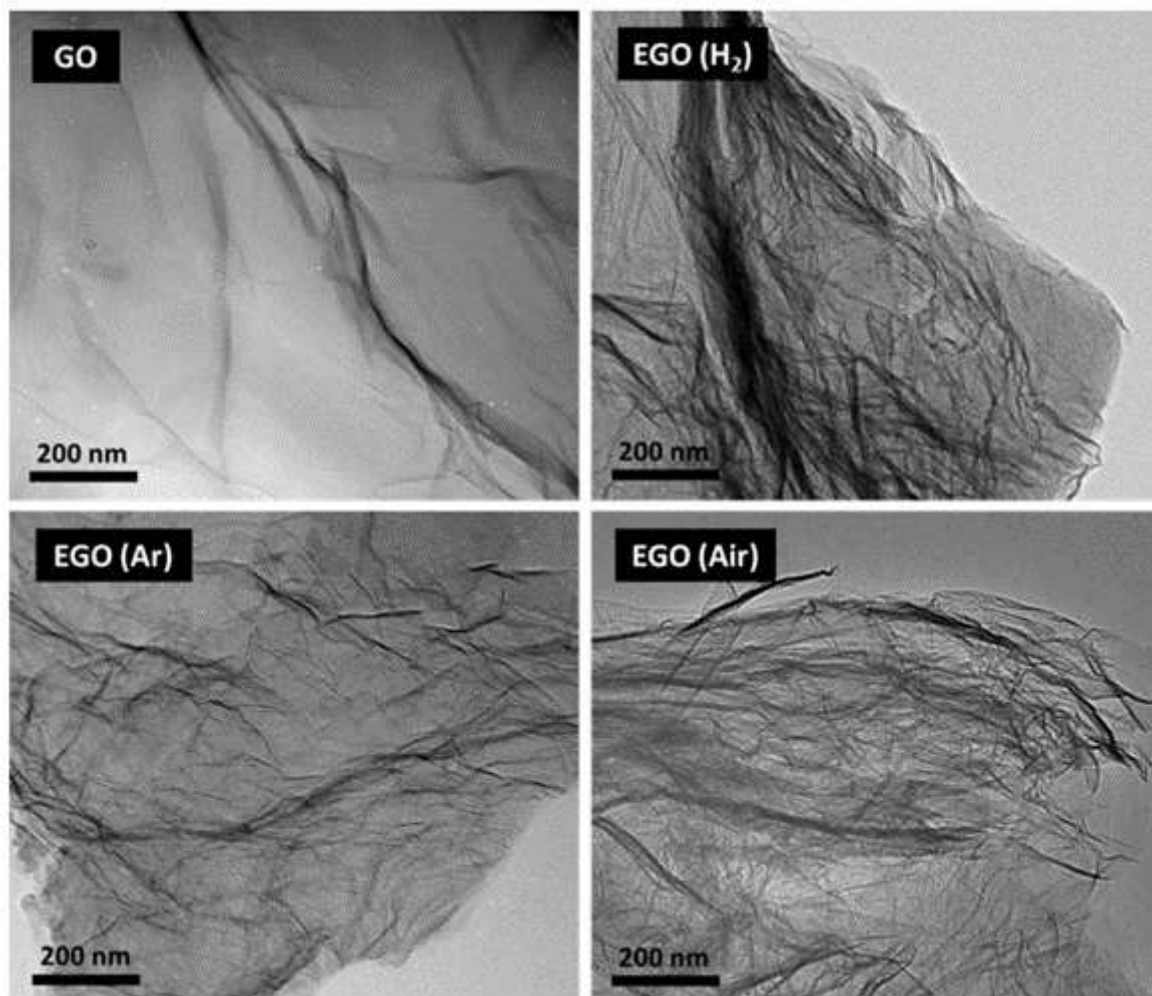


Figure 7

TEM images of graphite oxide (GO) and thermally exfoliated graphene oxide (EGO) samples in H₂, Ar or Air environments.

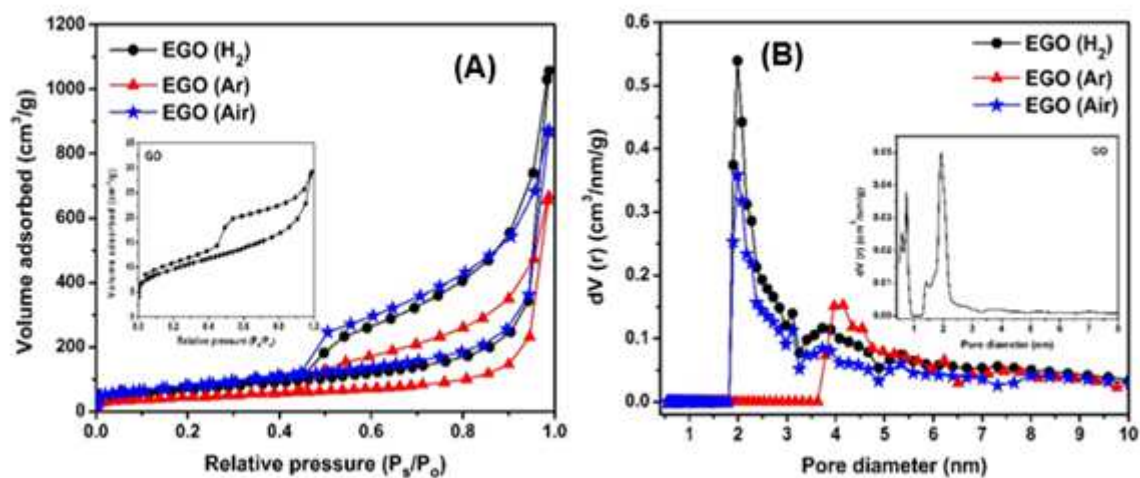


Figure 8

(A) N₂ adsorption–desorption isotherms (B) pore size distribution of graphite oxide (GO) and thermally exfoliated graphene oxide (EGO) samples in H₂, Ar or Air environments.

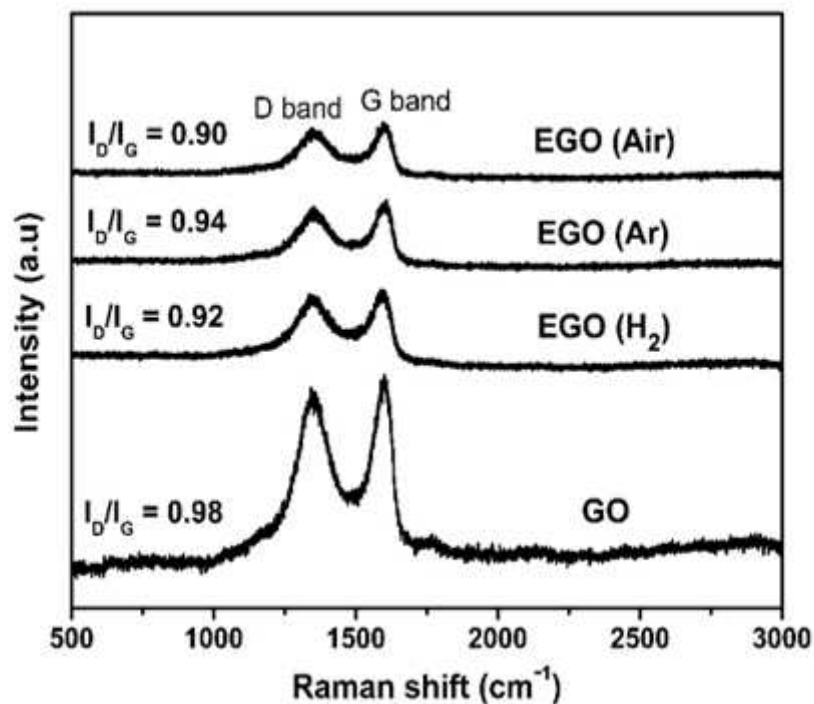


Figure 9

Raman spectra of graphite oxide (GO) and thermally exfoliated graphene oxide (EGO) samples in H₂, Ar or Air environments.

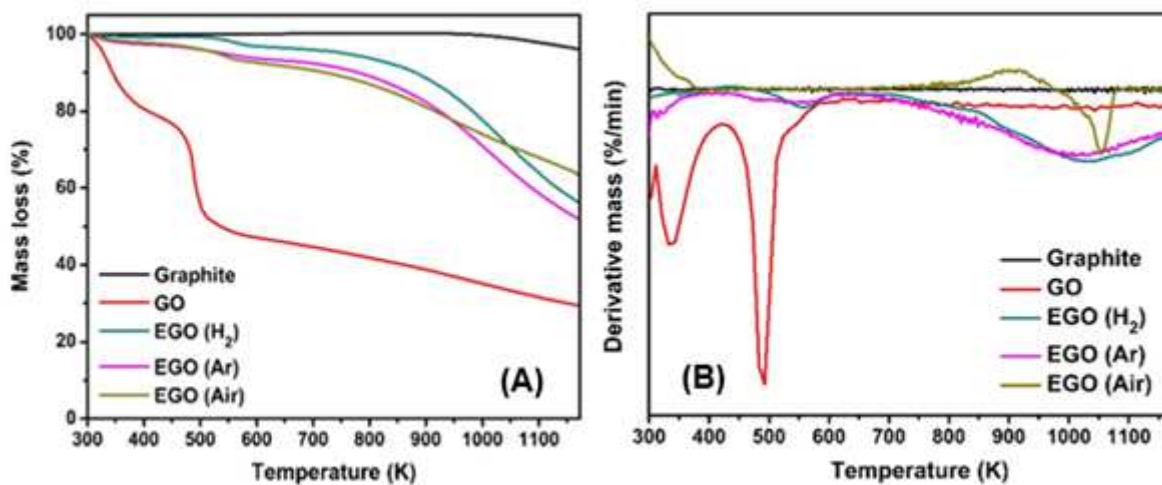


Figure 10

(A) Thermogravimetric analysis (TGA) (B) Differential Thermogravimetric (DTG) profiles of graphite, graphite oxide (GO) and thermally exfoliated graphene oxide (EGO) samples in H₂, Ar or Air environments.

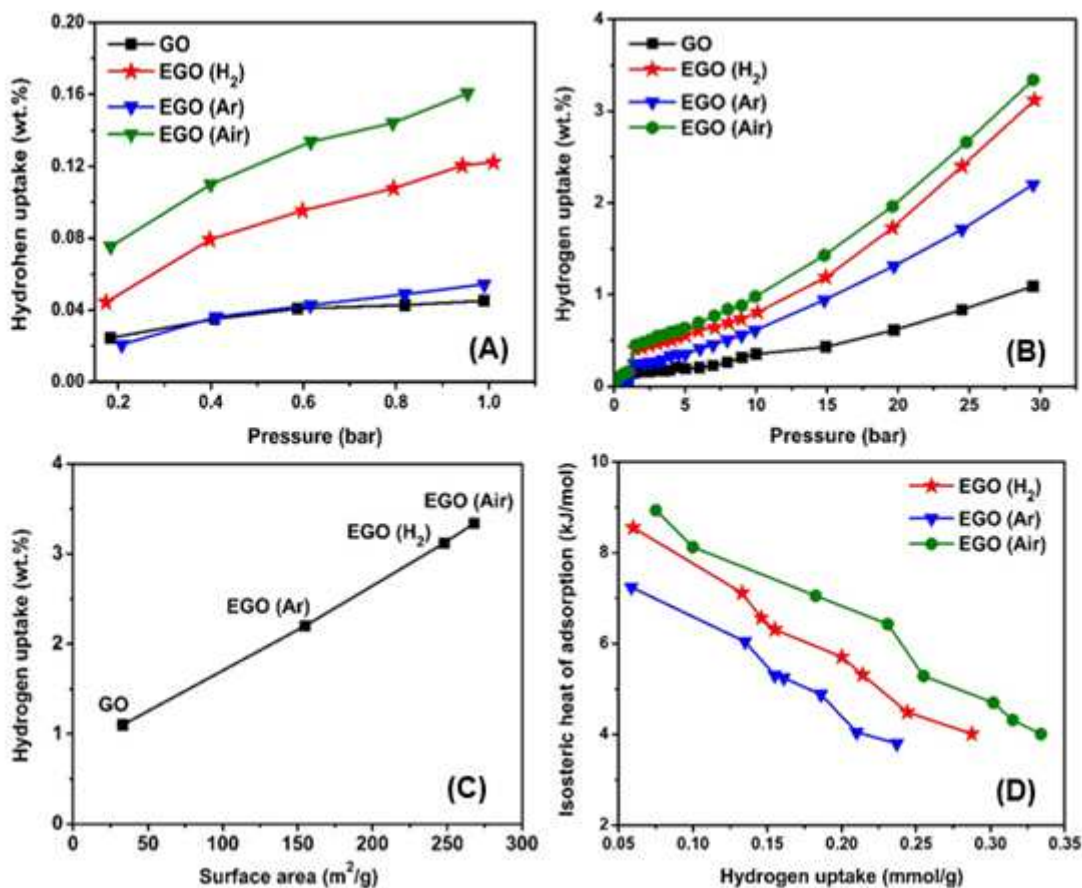


Figure 11

Hydrogen adsorption isotherms of samples at 77 K up to (A) 1 bar (B) 30 bar (C) Relation between hydrogen uptake capacity and surface area of the samples (D) Isosteric heat of adsorption as a function of the amount of H₂ adsorbed.

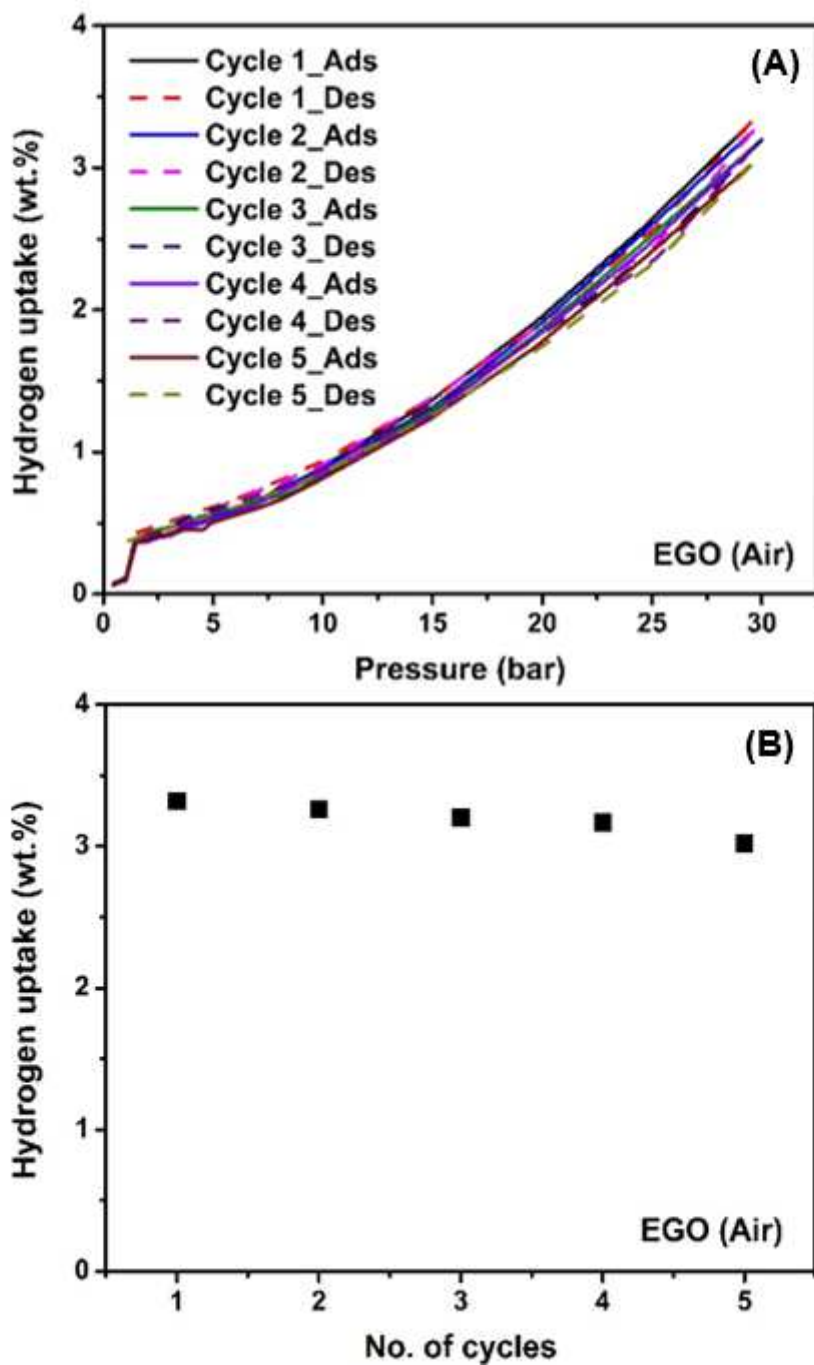


Figure 12

(A) Hydrogen adsorption-desorption isotherms of EGO (Air) at 77 K and 30 bar for five cycles (B) Cyclic stability for hydrogen uptake of EGO (Air) sample.

Supplementary Files

This is a list of supplementary files associated with this preprint. Click to download.

- [SupplementaryInformationRevised.docx](#)